**Article:**
Majiya, H, Adeyemi, OO orcid.org/0000-0002-0848-5917, Herod, M et al. (2 more authors) (2018) Photodynamic inactivation of non-enveloped RNA viruses. Journal of Photochemistry and Photobiology B: Biology, 189. pp. 87-94. ISSN 1011-1344

https://doi.org/10.1016/j.jphotobiol.2018.10.009

# Photodynamic inactivation of non-enveloped RNA viruses

Hussaini Majiya[1], Oluwapelumi O. Adeyemi[2], Morgan Herod[2], Nicola J. Stonehouse[2] and Paul Millner [1#]

[1]School of Biomedical Sciences, University of Leeds, UK

[2]School of Molecular and Cellular Biology, University of Leeds, UK

# Address correspondence to Paul Millner, P.A.Millner@leeds.ac.uk

**Key Words:** A-protein, MS2, bovine enterovirus, murine norovirus, singlet oxygen, TMPyP, photodynamic inactivation

**Abstract word count**: 131

**Text word count:** 7023

## Abstract

We recently reported the photodynamic inactivation (PDI) of bacteriophage MS2 with a photosensitiser- 5, 10, 15, 20-tetrakis (1-methyl-4-pyridinio) porphyrin- tetra- *p*-toluene sulfonate (TMPyP) in solution and concluded that the A-protein of the virus is the main target of inactivation. Here, we have extended these studies and carried out PDI of bacteriophage Qβ, bovine enterovirus 2 (BEV-2) and type 1 murine norovirus (MNV-1). The rate of inactivation observed was in the order MS2 > Qβ > MNV-1 > BEV-2. Data suggested that TMPyP-treatment could also target the viral genome as well as result in disintegration/disassembly of viral particles. Although emergence of viral drug resistance is a well-documented phenomenon, it was not possible to generate PDI-resistant MS2. However, emergence of a mutation in the lysis protein was detected after serial exposure to PDI.

## 1. Introduction

Photodynamic inactivation (PDI) of viruses has been shown to be a promising alternative antiviral strategy (Casteel et al., 2004, Pecson et al., 2012, Silverman et al., 2013, Wainwright, 2004, Costa et al., 2009, Costa et al., 2008, Costa et al., 2010). It is believed that Singlet oxygen and related reactive oxygen species (ROS) are responsible for the photodynamic inactivation of viruses (Costa et al., 2013). Among biomolecules, proteins have the highest bimolecular rate constant of singlet oxygen mediated oxidation ($10^5$ to $10^9$ $M^{-1}$ $S^{-1}$) followed by RNA ($10^4$ to $10^6$ $M^{-1}$ $S^{-1}$) (Davies, 2003, Cho et al., 2010). Singlet oxygen and other ROS can only cause damage to molecules in close proximity because of their high reactivity and short half-life (Costa et al., 2013). Therefore, capsid proteins including host recognition proteins are immediate targets of singlet oxygen mediated oxidation in non-enveloped viruses, while envelope glycoproteins, including host-recognition proteins, are potential targets of singlet oxygen oxidation in enveloped viruses. In some cases, these proteins also act as host-recognition proteins. However, capsid breathing of some non-enveloped viruses could allow small molecules into the capsid (Dedeo et al., 2010, Valegård et al., 1990, Adeyemi et al., 2017, Bothner et al., 2005, Jaegle et al., 1988, Jimenez-Clavero et al., 2000, Lewis et al., 1998, Pulli et al., 1998). This means that the viral genome could also be a target of PDI. Singlet oxygen can interact with potential targets either by physical quenching (which is only observed in tryptophan) and/or by chemical modification, which is observed in almost all amino acids. The chemical modification usually results in irreversible changes in amino acids with tryptophan, histidine, methionine, cysteine and tyrosine being most susceptible to singlet oxygen oxidation (Davies, 2003).

RNA viruses have high mutation rates that increases diversity within their populations and provides an enabling environment for adaptation (Duffy et al., 2008, Lauring et al., 2013, Domingo et al., 1996, Sanjuan et al., 2010, Irwin et al., 2016). Studies have reported on the emergence of resistant viruses upon continuous administration of antiviral drugs and exposure to common water disinfectants e.g. resistance of HIV to antiretroviral drugs (Hué et al., 2009), influenza virus to oseltamivir (Foll et al., 2014), hepatitis C virus to ribavirin (Feigelstock et al., 2011), bacteriophage MS2 and human echovirus 11 to chlorine dioxide ($ClO_2$) (Zhong et al., 2016, Zhong et al., 2017), poliovirus and bacteriophage F116 to free chlorine (Bates et al., 1977b, Payment et al., 1985) and human echovirus 11 to Ultraviolet C (UVC) (Carratalà et al., 2017).

Previously, we reported that a minimum dose of 0.2 µM TMPyP in solution under light (32 mW $cm^{-2}$) inactivated MS2 within one minute (Majiya et al., 2017). We also showed that the A-protein of MS2 was the PDI target and aggregation of the viral particles after sixty minutes of PDI treatment (Majiya et al., 2018). Although MS2 remains a useful and relevant virus for study, it is also necessary to investigate human (or closely related animal) viruses to accurately model inactivation of human viruses under relevant experimental conditions. A total of four non-enveloped, single strand positive sense RNA viruses were studied here (i.e. bacteriophages MS2 and Qβ, bovine enterovirus type-2 (BEV-2) and type 1 murine norovirus (MNV-1)). Common among these viruses are 27-35 nm icosahedral capsids that include the most susceptible residues to ROS- mediated oxidation (Figure 1A), thereby making the viral capsids possible PDI targets.

The MS2 capsid is made up of 178 copies of the coat protein (13.7 KDa) and one copy of the maturation or A-protein with which it binds the host bacterial pilus during infection (44 KDa)

(Dai et al., 2017, Koning et al., 2016). After-replication and assembly, the lysis protein allows the release of progeny virions from the infected cell (Walderich et al., 1988). The capsid of Qβ is also composed of 178 copies of coat protein (13.7 KDa) and one copy of maturation protein (referred to as the A2-protein) which participates in host bacteria cell recognition and attachment to the bacterial pilus during infection (Gorzelnik et al., 2016). However, unlike MS2, It has been shown that coat protein subunits of Qβ are linked by disulphide bonds to form covalent pentamers and hexamers (Takamatsu and Iso, 1982). The capsid of BEV-2 comprises 60 copies each of VP1 (34 KDa), VP2 (29 KDa), VP3 (27 KDa) and VP4 (7 KDa) (Smyth et al., 1995, Goens et al., 2004). VP1, VP2 and VP3 are exposed on the surface of the capsid while VP4 is internal and myristylated at its N-terminal residue (Kaminaka et al., 1999, Smyth et al., 1995). The host attachment sites of BEV-2 are on the surface ridge, analogous to the canyon described in polioviruses and rhinoviruses (Smyth et al., 1995). MNV-1 capsids are formed from 180 copies of VP1 together with a small, but uncharacterised number of VP2 proteins. Each copy of VP1 is divided into an N-terminal arm (N), a shell (S), and C-terminal protruding (P) domain (Taube et al., 2010, Katpally et al., 2010). The S and P domains are connected by a short hinge. The P domain forms arch-like dimers protruding from the capsid surface. It is subdivided into P1 (stem of the arch) and P2 (top of the arch) domains (Taube et al., 2010).

To date, although there are several studies on the adaptation of viruses to antiviral drugs and disinfectants as well as the adaptation of gram-positive and gram-negative bacteria to sub-lethal PDI conditions (Amin et al., 2016, Cassidy et al., 2010, Giuliani et al., 2010, Pourhajibagher et al., 2016a, Pourhajibagher et al., 2016b, Tavares et al., 2010, Zhang et al., 2014), there are few reports on viral adaptation to PDI-treatment (Costa et al., 2011). There

is therefore a need for investigations of viral adaptation to PDI to inform decision, choice and design of PDI as an alternative antiviral agent.

In this work, PDI-treatment of Qβ, MNV-1 and BEV-2 were investigated using TMPyP in solution, while adaptation of MS2 to PDI was investigated at sub-lethal doses. Additionally, effects of PDI-treatment on encapsidated viral RNA was investigated using MNV-1.

## 2. Material and methods

### *2.1 Light source, photosensitiser-TMPyP and conditions for PDI*

A Schott KL 2500 LCD (Schott Ltd., Stafford, UK), which provides a cool white light in the visible region of the spectrum (Figure 1B) was applied as the light source for the PDI experiments. The spectral properties of the light source was determined using a QE Pro, high sensitivity spectrometer, (Ocean Optics, USA). Fluence rates of illumination during photoinactivation experiments were measured using a light meter (Clas Ohlson, UK). Photosensitiser-TMPyP which has peak absorption within the visible region of the spectrum (Figure 1C) was purchased without further purification from Sigma Aldrich. Absorption spectra of TMPyP in phosphate buffered saline (PBS) (10 mM $Na_2HPO_4$, 1.8 mM $KH_2PO_4$, 137 mM NaCl, and 2.7 mM KCl) was determined using a NanoDrop $2000_C$ micro-spectrometer (Thermo Scientific) at 20-22 $^oC$ under aerobic conditions and a light intensity of 32 mW $cm^{-2}$.

### *2.2 Virus strains and their host cells*

Stocks of bacteriophage MS2 and Qβ and their *E. coli* host cells were a gift from Prof. P. Stockley University of Leeds, UK. Bovine enterovirus 2 (BEV-2) were provided by Prof. D. Rowlands, University of Leeds, UK. The murine norovirus (MNV-1), RAW 264.7 cells and rabbit anti-MNV capsid protein (VP1) polyclonal antibodies used in this study were kindly provided by Prof. I. Clarke (University of Southampton, UK). BL21 *E. coli* and BHK-21 cells were from standard laboratory stocks and rabbit anti-MS2 virus polyclonal antibodies were sourced commercially from Genscript, USA.

### *2.3 Propagation and purification of bacteriophages MS2 and Qβ*

The bacteriophages MS2 and Qβ were propagated in *E. coli* and purified as previously described (Majiya et al., 2018).

### *2.4 Propagation and purification of BEV-2*

BHK-21 cells were grown to 80-90% confluence according to standard procedures. Cells were infected with BEV-2 and incubated at 37 $^{o}$C under 5% $CO_2$ for 48 hours. Cells were lysed by freeze-thaw cycles and clarified by centrifugation at 1,431 xg for 10 minutes. Virus particles in the supernatant were precipitated using 50% (v/v) saturated ammonium sulphate at 4 $^{o}$C overnight. The precipitate was pelleted by centrifugation at 1,430 xg for 30 minutes and re-suspended in 10 ml PBS. Following a clarification step by centrifugation at 1,430 x g for 10 minutes, supernatant was concentrated through a 30% (w/v) sucrose cushion by ultracentrifugation at 175,000x g for 3 hours using a Beckman SW 32 Ti rotor. The pellet was re-suspended in PBS and the virus purified through a 15–45% (w/v) sucrose gradient by ultracentrifugation at 160,000 x g for 2 hours using a Beckman SW 40 Ti rotor. Gradient fractions were collected from top to bottom and virus peak fractions were determined by SDS-PAGE (Weber and Osborn, 1969) followed by western blotting (Liu et al., 2014) using standard protocols.

### *2.5 Propagation and purification of MNV-1*

RAW 264.7 cells were grown to 70-80% confluence according to standard procedures. Cells were infected with MNV-1 and incubated at 37 $^{o}$C under 5% $CO_2$ for 72 hours. Cells were lysed by freeze-thaw cycles and clarified three times by centrifugation at 1,431 xg for 10 minutes. The supernatant was harvested and virus particles concentrated through a 30% (w/v) sucrose cushion by ultracentrifugation at 175,000 xg for 3 hours using a Beckmann SW 32 Ti rotor.

The supernatant was discarded and pellet re-suspended in PBS. Re-suspended pellet was clarified by centrifugation at 13,000 rpm for 10 minutes and purified through a 15-60% sucrose gradient by ultracentrifugation at 300,000 xg for 50 minutes using a Beckmann SW 55 Ti rotor. Gradient fractions were collected from top to bottom and virus peak fractions were determined by SDS-PAGE (Weber and Osborn, 1969) followed by immunoblotting against anti-MNV-1 VP1 using standard protocols (Liu et al., 2014).

### 2.6 *Photodynamic inactivation (PDI) of viruses*

A range of concentrations of TMPyP from 0.5 µM to 50 µM was applied at a light intensity of 32 mW $cm^{-2}$ for durations of illumination ranging from 10 seconds to 120 minutes. As controls, a dark experiment (D) was carried out in the presence of photosensitizer but without illumination, while "no sensitiser" (NS) experiments were exposed to light but in the absence of photosensitiser. All experiments were repeated in triplicate.

### *2.7 RNA transfection*

To assess the effect of PDI on the MNV genome, the RNA of TMPyP-treated MNV samples were extracted and purified using commercial Direct-Zol Miniprep Plus kits. Purified RNA was transfected into BHK-21 cells using Lipofectin reagent according to the recommended protocol. Transfected cells were incubated at 37$^{o}$C under 5% $CO_2$ for 48 hours.

### *2.8 Virus titration assays*

To determine titre of bacteriophages MS2 and Qβ, double layer agar plaque assays were undertaken according to standard methods (Kropinski et al., 2009). To determine titre of BEV-2, virus titres were determined by plaque assays were also used according to standard

procedures (Dulbecco and Vogt, 1954), while MNV titres were determined by $TCID_{50}$ assays (Reed and Muench, 1938).

### *2.9 Transmission electron microscopy*

TMPyP-treated and non-treated samples were each dialysed into buffer (10 mM Hepes, 100 mM NaCl, 1.27 mM EDTA). Sample dialysates were negatively stained with 1% (w/v) uranium acetate and analysed by transmission electron microscopy according to standard methods (Humphrey, 2008, Stonehouse and Stockley, 1993).

### *2.10 MS2 PDI and evolution experiment*

Our previously used and reported PDI conditions of 0.5 µM TMPyP, 32 mW $cm^{-2}$ and 30 sec illumination at 32 mW $cm^{-2}$ which resulted to reductions of 4 log PFU/ml of MS2 from an initial titre of 9.6 log PFU/ml was used to select about 5 log PFU/ml of the MS2 populations still viable (Majiya et al., 2017). In order to test whether MS2 could evolve into PDI-resistant MS2, the viable populations were selected and then subjected to repeated cycles of same PDI conditions until the $10^{th}$ cycle. After each treatment cycle, virus titres were determined by double layer agar plaque assays before and after TMPyP PDI-treatment.

### *2.11 Viral genome extraction and sequencing*

In order to identify genetic changes, viral RNA was extracted and purified using Direct-Zol Miniprep Plus kits. Purified RNA genome was reverse-transcribed into cDNA using the SuperScript II commercial kit according to manufacturer's protocol. The cDNA was amplified by PCR using high fidelity Phusion® DNA polymerase (New England Biolab, UK) with a set primer of forward and reverse primers that covered the full genome of MS2. PCR products were purified using a Qiagen DNA gel extraction kit according to manufacturer's protocol and sequenced using genomic primers. PCR products were cloned into transient vector, pCRBlunt

(Thermo fisher Scientific, USA) according to manufacturer's protocol. Plasmid was transformed into DH5α *E. coli* cells and propagated in the presence of kanamycin. Colonies were screened for inserts by diagnostic digest using restriction-enzyme, *EcoR*I (New England Biologicals #3101). Positive colonies that contained the cloned inserts were sequenced using genomic primers. Primer sequences are available on request.

# 3. Results

## *3.1 Abundance of PDI-susceptible residues on viral capsids*

PDI is a promising alternative antiviral strategy against enveloped (Käsermann and Kempf, 1997) and non-enveloped viruses (Silverman et al., 2013). Studies have suggested that amongst the amino acids, tryptophan, histidine, methionine, cysteine and tyrosine are most susceptible to singlet oxygen mediated oxidation under physiological pH conditions (Davies, 2003, Wilkinson et al., 1995, Gracanin et al., 2007). However, the abundance of these amino acids varies among viral capsid proteins. We therefore speculated that virus susceptibility to TMPyP-PDI may be a function of the abundance of these residues on the viral capsid as well as the singlet oxygen-accessibility to these residues. Estimating the abundance of these susceptible residues on the capsids of the viruses studied here, showed that MNV-1, MS2, BEV-2 and bacteriophage Qβ possessed these susceptible amino acids in varying abundance (Figure 1A).

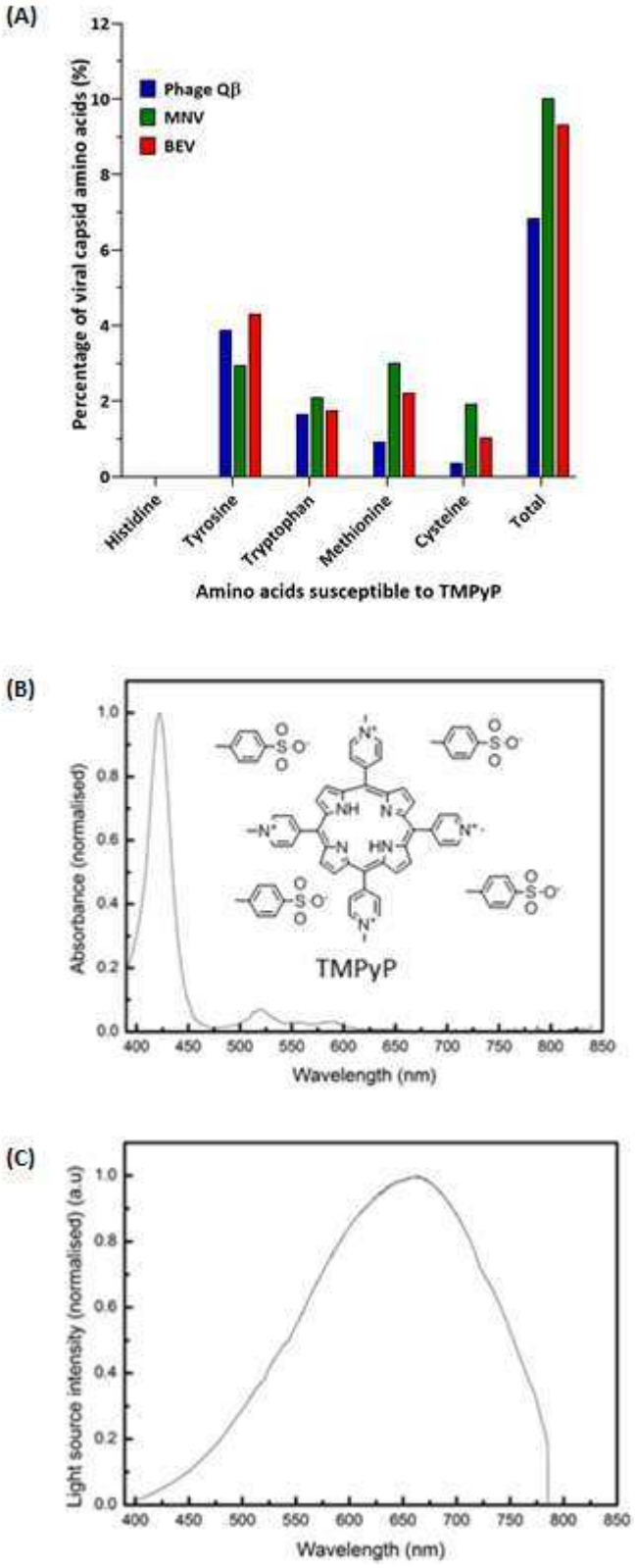


**Figure 1: Spectral properties of PDI light source and absorption spectra of TMPyP, and amino acids most susceptible to singlet oxygen mediated oxidation among model viruses.** (A) Percentage of the capsid protein residues that are most susceptible to PDI among the icosahedral viruses studied. Reference sequences of bacteriophages MS2 (NC_001417.2), and Qβ (AY099114.1), MNV-1 (KR349276.1) and BEV-2 (AY508697.1) were accessed from the NCBI

genebank and assessed for abundance of tryptophan, histidine, methionine, cysteine and tyrosine within the capsid region. Figure also shows the percentage abundance of a combination of all five amino acids susceptible to singlet oxygen mediated oxidation. (B), light spectra of our PDI light source (Schott KL 2500 LCD, Schott Ltd., UK). The PDI light source spectra (400 nm – 786 nm) showed that this mainly emitted visible light including some near infrared. The spectral peak is between 641 nm - 661 nm; (C), absorption spectra of the photosensitiser-TMPyP used for PDI of the viruses. The absorption peak of TMPyP is 422 nm. The TMPyP chemical structure was from ChemACX.com, ChemDraw Pro 13.0.

### *3.2 PDI-treatment of Phage Qβ, BEV-2 and MNV-1*

Previously, we showed that 0.5 µM TMPyP solution under illumination with light intensity of 32 mW $cm^{-2}$ caused complete inactivation of MS2 within 1 min (Majiya et al., 2017). Using these and other PDI conditions, we investigated the PDI of representative icosahedral viruses of the families *Leviviridae* (Qβ), *Picornaviridae* (BEV-2) and *Caliciviridae* (MNV-1) as virus models to investigate mechanisms of PDI in non-enveloped viruses. Prior to PDI-treatment, the viruses were purified to prevent interference in PDI due to impurities that could quench the singlet oxygen (and other ROS) generated. In order to investigate PDI-inactivation of the viruses over time, purified virus samples were treated with up to 10 µM TMPyP and 32 mW $cm^{-2}$ light. Our data suggested that the complete inactivation of Qβ occurred after 8 minutes (Figure 2A). Some reduction in titre of MNV and BEV was observed but with much higher concentrations of TMPyP and for longer time periods (up to 120 minutes) (Figure 2B and C).

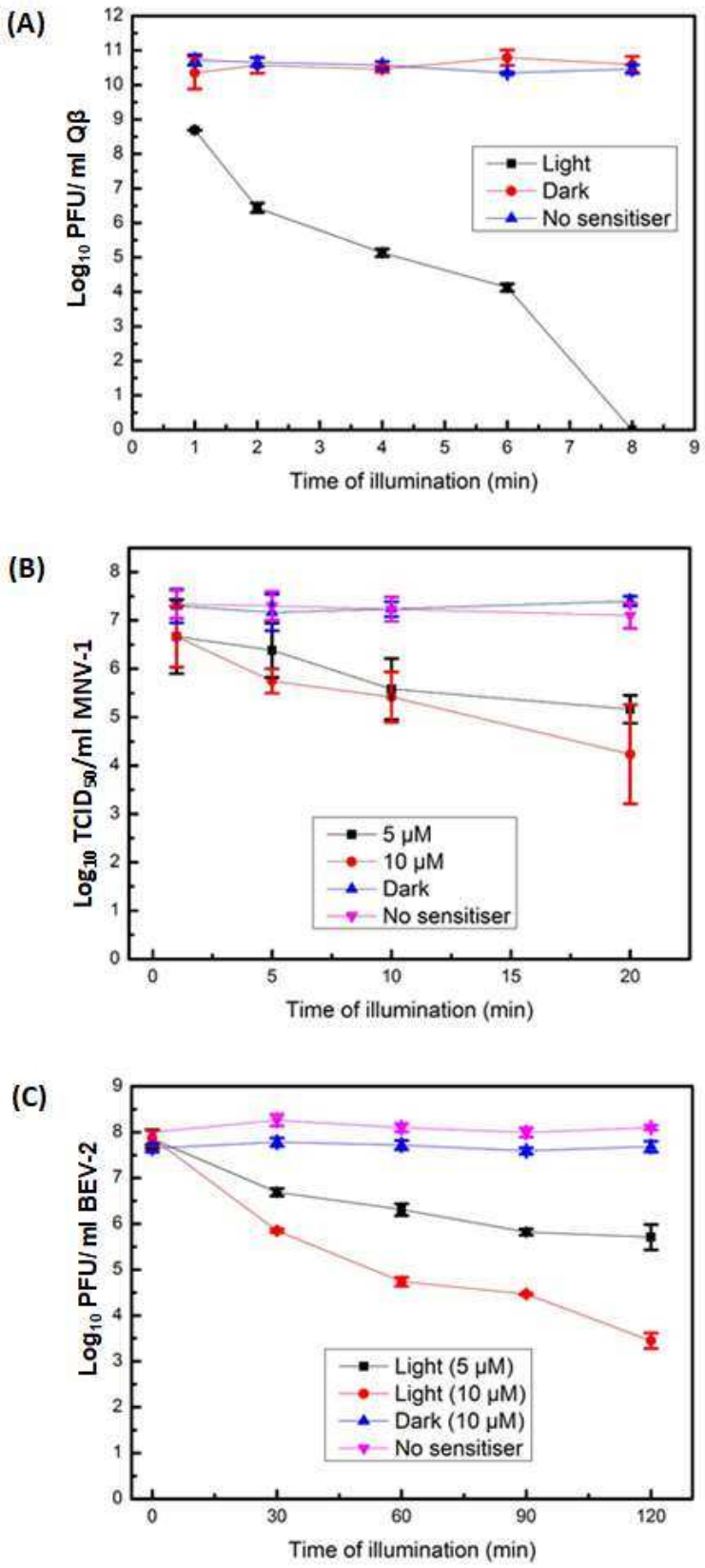


**Figure 2: PDI of icosahedral viruses over time.** The samples were and illuminated at 32 mW $cm^{-2}$. The figure shows PDI kinetics of (A), Qβ Virus samples treated with 0.5 µM TMPyP; (B), MNV-1 treated with 5 µM and 10 µM TMPyP; (C), BEV-2 treated with 5 µM and 10 µM TMPyP.

The dark controls were treated with the concentration of photosensitiser shown but not illuminated whilst no photosensitiser controls (NS) were illuminated without photosensitiser present. n = 3 ± S.D.

### *3.3 Effects of TMPyP-PDI on capsid integrity*

Previously, we showed that TMPyP-PDI may affect the integrity of the MS2 capsid and may result in aggregation of viral particles (Majiya et al., 2018). We therefore sought to investigate the structural effects of TMPyP PDI-treatment on the capsid integrity of other viruses using negative stain electron microscopy. Purified samples of Qβ, MNV-1 and BEV-2 were treated with 50 μM TMPyP for a range of durations from 1 minute to 60 minutes. Treated virus samples were negatively stained and viewed by TEM (Figure 3).

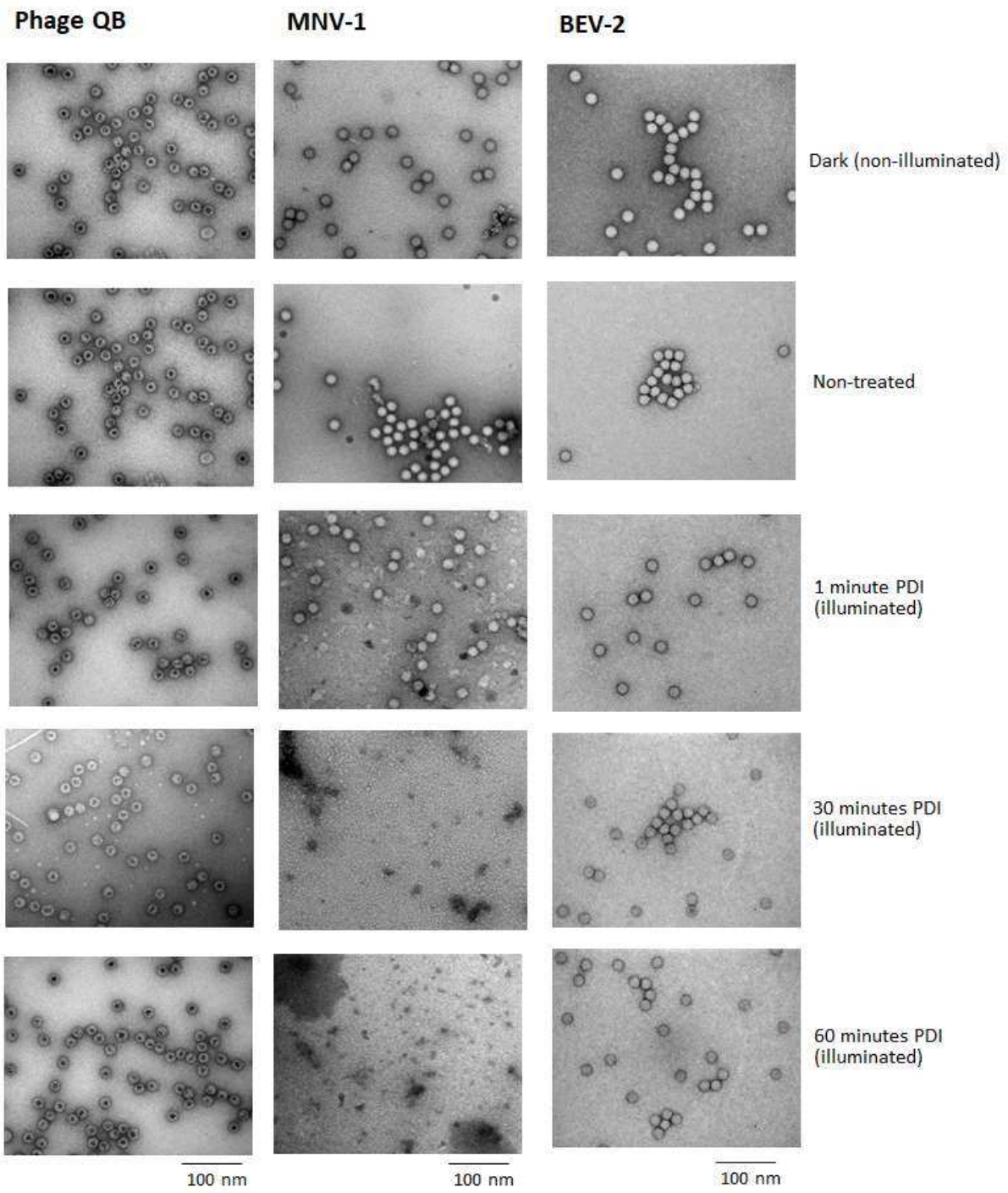


**Figure 3: TEM of PDI treated model viruses with 50 µM TMPyP in solution.** Samples of Qβ, MNV-1 and BEV-2 were purified through sucrose gradients and dialysed into TEM buffer as described in Methods. Dialysed virus samples were treated with 50 µM TMPyP and illuminated at 32 mW $cm^{-2}$ for a range of durations from 1 minute to 60 minutes. As controls, "Dark experiments" were also treated with 50 µM TMPyP but incubated for 60 minutes. Treated samples were immediately stained with 1% (w/v) uranyl acetate and visualised by TEM. Figure shows negatively stained TEM micrographs of Qβ, BEV-2 and MNV-1, respectively. Sample treatments are indicated on the right-hand panel. Scale bars are shown underneath each micrograph column.

Unlike previously reported aggregation of MS2 (Majiya et al., 2018), Qβ and BEV-2 did not show evidence of aggregation post- TMPyP PDI-treatment for up to 60 minutes. However, our data suggested some alterations to the appearance of the MNV-1 capsids following a short TMPyP PDI-treatment. Furthermore, no intact virions were detected after 30 minutes of PDI-treatment and it is possible that the capsids had disassembled/disintegrated.

### *3.4 Can the viral genome be affected by TMPyP-PDI?*

Owing to the capsid breathing phenomenon common to icosahedral viruses (Bothner et al., 2005, Lewis et al., 1998, Jaegle et al., 1988, Witz and Brown, 2001), we previously suggested that there could be effects of PDI on inner residues of the viral capsid protein and the viral genome (Majiya et al., 2018). Here, using MNV-1 as a study model, we sought to investigate the effect of PDI on the encapsidated viral genome. Samples of MNV-1 were PDI-treated as previously described. Post-treatment, the viral genome was extracted and purified. For RNA viruses, the genome alone is infectious when introduced into susceptible cells. This phenomenon allows the analysis of the effects of PDI on the genome in the absence of the capsid. Here, the purified genomic RNA from PDI-treated viruses was transfected into susceptible cells and titrated for infectivity (Figure 4).

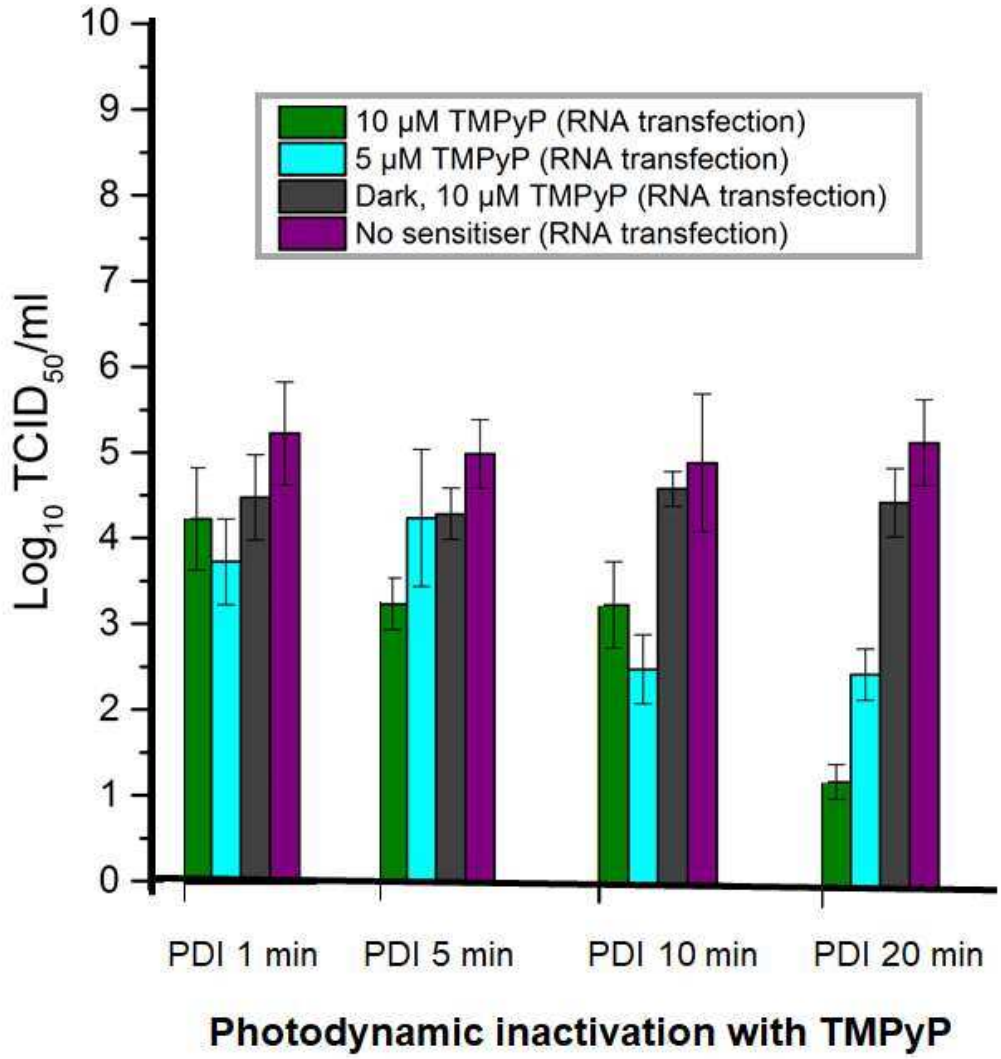


**Figure 4: The effect of TMPyP-PDI treatment on RNA infectivity of MNV-1.** Samples of MNV-1 were treated with 5 µM and 10 µM TMPyP and illuminated at 32 mW $cm^{-2}$ for up to 20 minutes. Viral RNA was extracted from these samples and transfected into RAW 264.7 cells. Recovered viral infectivity titres were determined by $TCID_{50}$ assays. As controls, "dark" samples were treated 10 µM TMPyP in the absence of light illumination, while "no sensitizer" samples (NS) were illuminated in the absence of TMPyP (n = 3 ± S.D.).

The average titre of the viruses used here was approximately 7.3 log $TCID_{50}$/ml (as shown in the data in Figure 2B). After RNA extraction, purification and transfection the titres were much reduced, as shown by the dark and no sensitizer control data in Figure 4. These loses were consistent throughout the experiment and suggest that the process viral RNA recovery,

as well as the transfection efficiency may have resulted to some loss of viral titres. However, RNA extracted from viruses that has been exposed to phototreatment with TMPyP yielded a further reduction in titre upon transfection. Furthermore, this decrease was dependent on both the TMPyP concentration and time of phototreatment (Figure 4). This demonstrates that PDI could also target the encapasidated viral genome of some viruses such as MNV-1.

### *3.5 Selecting for TMPyP-PDI -resistant MS2*

We have previously reported that 0.5 μM TMPyP under light intensity of 32 mW $cm^{-2}$ for 1 minute, resulted in total inactivation of MS2. Here, we attempted to select TMPyP PDI-resistant MS2 variants at this concentration but with light illumination for 30 seconds, which resulted to over 99.99% loss in viral titre (Majiya et al., 2017). After TMPyP-PDI treatment for 30 seconds, surviving MS2 virus populations were recovered by passage. Cycles of PDI-treatment followed by virus recovery were repeated for a total of ten cycles, and pre- and post-treated virus titres were determined by double layer agar plaque assays (Figure 5A). Viral RNA extracts from selection cycles 6 and 10 were reverse-transcribed, cloned into a transient vector (pCR-Blunt) and sequenced (Figure 5B).

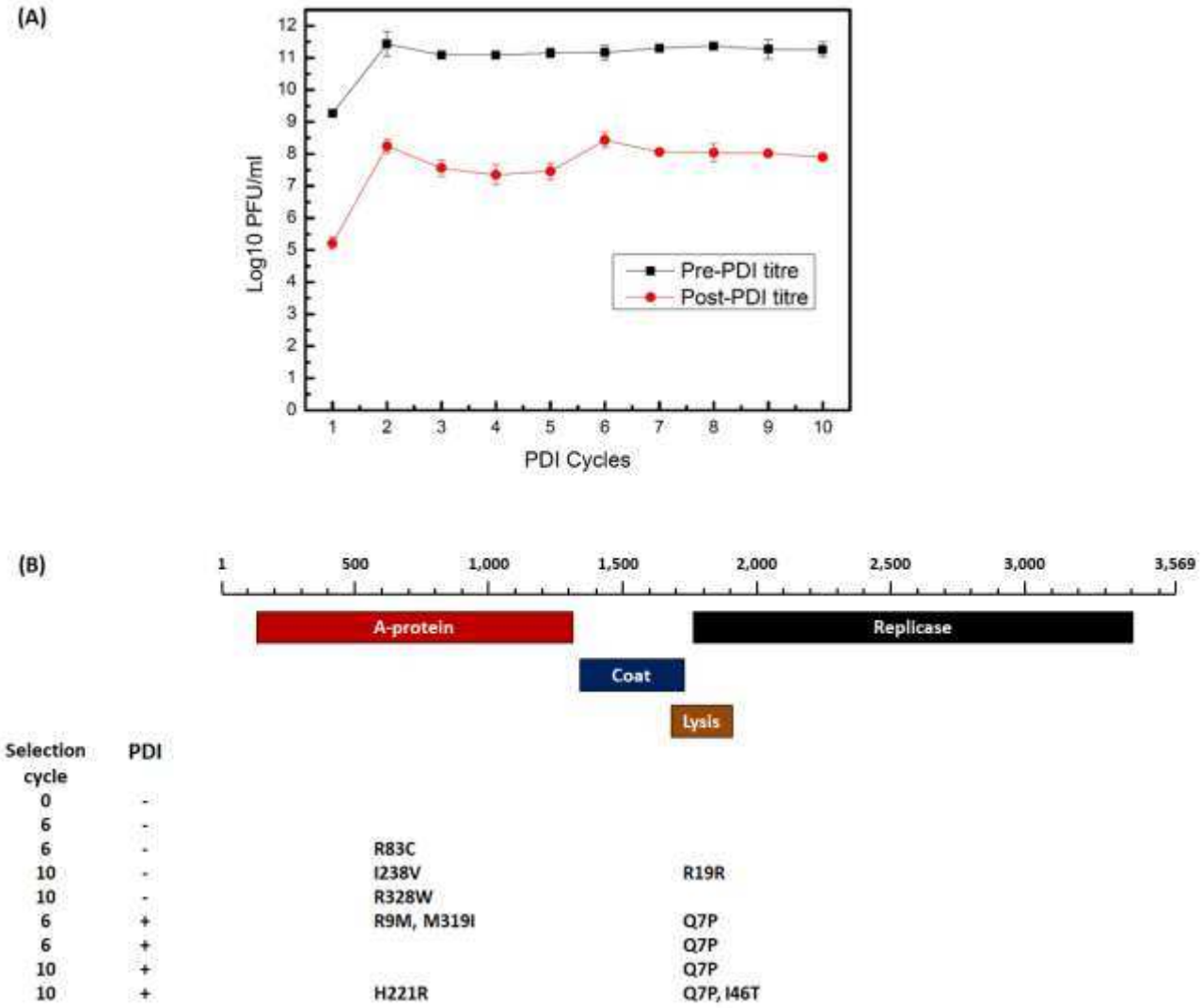


**Figure 5. Selection of PDI-resistant MS2**. (A) Figure shows infectivity titre of MS2 before and after TMPyP-PDI treatment. Each PDI cycle was subjected to 0.5 µM TMPyP and illuminated at 32 mW.cm$^{-2}$ for 30 seconds. As a control, a sample of MS2 was passaged serially in the absence of TMPyP for 10 cycles (n = 3±S.D.). (B) Viral genomic RNA was extracted from recovered passages 0, 6 and 10. RNA was reverse-transcribed into cDNA and cloned into transient vector pCR-Blunt. Colony clones of individual genomes of wild-type, TMPyP-PDI treated and non-treated cycle passages 6 and 10 were purified and sequenced. Sequence reads were aligned against reference MS2 sequence (NC_001417.2). Figure shows a cartoon annotation of the MS2 (NC_001417.2) genome. The cartoon shows open reading frames (ORFs) of the A-protein (red), coat protein (blue), lysis protein (green) and replicase (black). Mutations identified are listed below respective open reading frames. The mutation at nucleotide 1,697 resulted to a synonymous coat protein mutation (S121S), and a non-synonymous lysis protein mutation (Q7P).

Throughout the PDI cycles, we consistently observed reductions of ~4 $\log_{10}$ PFU/ml over the 10 cycles which indicates that no significant resistance to PDI had emerged in the MS2 population (Figure 5A). Following selection, no phenotypic changes were observed. Despite this, we sought to investigate the occurrence of mutations at the genomic level within the population under selection and control viruses, passaged in the presence and absence of TMPyP selection. The 3.6 kbp MS2 genome encodes for a maturation protein (A-protein), coat protein, lysis protein and replicase (Figure 5B). Nucleotide changes were observed in both populations of viruses, as expected for RNA viruses. We will focus on the mutations that resulted in amino acid changes here. One of the viruses serially passaged in the absence of TMPyP-PDI treatment had a mutation in the A-protein (R83C, at the 6$^{th}$ passage). A different A-protein mutation (I238V) was observed in one of the viruses at the 10$^{th}$ passage, with R328W observed in a second virus (Figure 5B). Mutations R9M, M319I and H221R, also resulting in coding changes in the A protein, were observed in the PDI-treated viruses. None of the viruses sequenced had coding changes in the coat protein. However, because the lysis protein is produced in frameshift, non-synonymous mutations in the coat protein gene can result in lysis protein mutations. Indeed, a Q7P mutation was detected for all of the PDI-treated viruses. (Figure 5B).

## 4. Discussion

The viruses used in this study have structural and genomic similarities being lytic, non-enveloped, positive sense and single stranded RNA viruses with 27-35 nm icosahedral capsids. They have been employed as model organisms for this group of viruses in general. Furthermore, being members of the same family *Leviviridae*, MS2 and Qβ share host bacteria

for replication. Despite these similarities, the rates of inactivation and physical changes to capsids, as induced by PDI, varied.

Studies have shown that the rate and extent of inactivation of microorganisms is dose-dependent on photosensitiser and duration of exposure (Casteel et al., 2004, Costa et al., 2008, Costa et al., 2010, Costa et al., 2012). The leviviriruses (MS2 and Qβ) were the most susceptible to TMPyP PDI, respectively, followed by the calicivirus (MNV-1), while the picornavirus (BEV-2) was least susceptible to the TMPyP PDI-treatment. It is noteworthy that unlike MS2, the capsids of Qβ have disulphide linkages (Takamatsu and Iso, 1982) that could contribute to the slower rate of inactivation as compared to MS2. It is also possible that lack of aggregation and or disintegration of Qβ particles even after 60 minutes PDI-treatment could be due to the stability conferred on its capsid by the disulphide linkages. While MNV-1 particles disintegrated under TMPyP-PDI treatment, we could not detect physical differences between the TMPyP-PDI treated and non-treated BEV-2 or Qβ particles by the transmission electron microscopy here. Additionally, the abundance of TMPyP PDI-susceptible amino acids on the capsid may play contributory roles if readily accessible. The lack of aggregation or disintegration of Qβ or BEV particles post-PDI treatment may have been influenced by their net surface charge. However, residues such as histidine, tryptophan and tyrosine are known to crosslink proteins when oxidised by singlet oxygen. (Davies, 2003, Shen et al., 2000b, Shen et al., 2000a, Carroll et al., 2017). Also, in some instances, secondary dark reactions have been implicated in the formation of protein crosslinks (Davies, 2003).

RNA viruses rapidly evolve and therefore viruses with resistance to antiviral agents and disinfectants can arise when viruses are repeatedly exposed to sub-lethal doses of these agents (Carratalà et al., 2017, Bates et al., 1977a, Feigelstock et al., 2011, Foll et al., 2014, Hué

et al., 2009, Irwin et al., 2016, Zhong et al., 2016, Zhong et al., 2017). PDI is an efficient antiviral agent for viral control, with only one study reporting an attempt to select PDI-resistant viruses (Costa et al., 2011). Our unsuccessful attempt to select for TMPyP-PDI-resistant MS2 agrees with the previously reported study as to the lack of emergence of PDI-resistant viruses (Costa et al., 2011) and bacteria (Zhang et al., 2014, Tavares et al., 2010, Pourhajibagher et al., 2016b, Pourhajibagher et al., 2016a, Giuliani et al., 2010, Cassidy et al., 2010). However, within the quasi-species population of viruses sequenced in this study, some mutations identified within the A-protein (i.e. I238V, and R9M) as well as the lysis protein have been previously reported as conferring resistance against $ClO_2$ following repeated exposure to this disinfectant (Zhong et al., 2016). Since the MS2 lysis protein is essential to viral egress through the induction of host-cell lysis (Walderich et al., 1988), the emergence of the lysis protein mutation (Q7P) (Zhong et al., 2016) among TMPyP-PDI selected viruses suggests that sub-lethal doses of TMPyP in solution could target other stages of the viral life cycle. However, as no resistant viruses were selected, it is also possible that the mutations did not arise as a result of TMPyP treatment.

## 5. Conclusion

The results obtained in this work has shown that the chief determinant of rate and extent of PDI among viruses are the structure, amino acid composition and surface/solvent accessibility of their host attachment proteins/sites. This is at least true in non-enveloped viruses. Capsid proteins especially host attachment proteins/sites could be immediate targets of singlet oxygen oxidation in non-enveloped viruses such our model viruses. Therefore, the rate and extent of PDI of our model viruses with TMPyP in solution in the order MS2 > Qβ > MNV > BEV, could be attributable in part to the abundance of amino acids that are susceptible to

singlet oxygen mediated oxidation and the solvent accessibility to these amino acids, together with possible effects on the RNA genome. Although selection of adaptive mutations were observed in this study, it was encouraging to note that MS2 resistance to PDI was not observed throughout the 10 PDI cycles. However, further investigation would be required to confirm these observations.

## Acknowledgements

This work was supported by Petroleum Technology Development Fund (PTDF) (PTDF/E/OSS/PHD/MHM/644/14), Nigeria. The authors would also like to thank members of the Millner and Stonehouse research groups at the University of Leeds, UK.

# References


ADEYEMI, O. O., NICOL, C., STONEHOUSE, N. J. & ROWLANDS, D. J. 2017. Increasing type 1 poliovirus capsid stability by thermal selection. *Journal of Virology,* 91**,** e01586-16.

AMIN, R. M., BHAYANA, B., HAMBLIN, M. R. & DAI, T. 2016. Antimicrobial blue light inactivation of Pseudomonas aeruginosa by photo-excitation of endogenous porphyrins: In vitro and in vivo studies. *Lasers in Surgery and Medicine,* 48**,** 562-568.

BATES, R. C., SHAFFER, P. T. & SUTHERLAND, S. M. 1977a. Development of poliovirus having increased resistance to chlorine inactivation. *Applied and Environmental Microbiology,* 34**,** 849.

BATES, R. C., SHAFFER, P. T. B. & SUTHERLAND, S. M. 1977b. Development of Poliovirus Having Increased Resistance to Chlorine Inactivation. *Applied and Environmental Microbiology,* 34**,** 849-853.

BOTHNER, B., TAYLOR, D., JUN, B., LEE, K. K., SIUZDAK, G., SCHLUTZ, C. P. & JOHNSON, J. E. 2005. Maturation of a tetravirus capsid alters the dynamic properties and creates a metastable complex. *Virology,* 334**,** 17-27.

CARRATALÀ, A., SHIM, H., ZHONG, Q., BACHMANN, V., JENSEN, J. D. & KOHN, T. 2017. Experimental adaptation of human echovirus 11 to ultraviolet radiation leads to resistance to disinfection and ribavirin. *Virus evolution,* 3**,** vex035.

CARROLL, L., PATTISON, D. I., DAVIES, J. B., ANDERSON, R. F., LOPEZ-ALARCON, C. & DAVIES, M. J. 2017. Formation and detection of oxidant-generated tryptophan dimers in peptides and proteins. *Free Radical Biology and Medicine,* 113**,** 132-142.

CASSIDY, C. M., DONNELLY, R. F. & TUNNEY, M. M. 2010. Effect of sub-lethal challenge with Photodynamic Antimicrobial Chemotherapy (PACT) on the antibiotic susceptibility of clinical bacterial isolates. *Journal of Photochemistry and Photobiology B: Biology,* 99**,** 62-66.

CASTEEL, M. J., JAYARAJ, K., GOLD, A., BALL, L. M. & SOBSEY, M. D. 2004. Photoinactivation of hepatitis A virus by synthetic porphyrins. *Photochemistry and Photobiology,* 80**,** 294-300.

CHO, M., LEE, J., MACKEYEV, Y., WILSON, L. J., ALVAREZ, P. J. J., HUGHES, J. B. & KIM, J. H. 2010. Visible Light Sensitized Inactivation of MS-2 Bacteriophage by a Cationic Amine-Functionalized C-60 Derivative. *Environmental Science & Technology,* 44**,** 6685-6691.

COSTA, L., ALVES, E., CARVALHO, C. M. B., TOME, J. P. C., FAUSTINO, M. A. F., NEVES, M. G. P. M. S., TOME, A. C., CAVALEIRO, J. A. S., CUNHA, A. & ALMEIDA, A. 2008. Sewage bacteriophage photoinactivation by cationic porphyrins: a study of charge effect. *Photochemical & Photobiological Sciences,* 7**,** 415-422.

COSTA, L., CARVALHO, C. M. B., FAUSTINO, M. A. F., NEVES, M. G. P. M. S., TOME, J. P. C., TOME, A. C., CAVALEIRO, J. A. S., CUNHA, A. & ALMEIDA, A. 2010. Sewage bacteriophage inactivation by cationic porphyrins: influence of light parameters. *Photochemical & Photobiological Sciences,* 9**,** 1126-1133.

COSTA, L., CARVALHO, C. M. B., TOME, J. P. C., FAUSTINO, M. A. F., NEVES, M. G. P. M. S., TOME, A. C., CAVALEIRO, J. A. S., LIN, Z., RAINHO, J. P., ROCHA, J., CUNHA, A. & ALMEIDA, A. 2009. Sewage bacteriophage photoinactivation by porphyrins immobilized in solid matrixes. *Current Research Topics in Applied Microbiology and Microbial Biotechnology***,** 338-341.

COSTA, L., FAUSTINO, M. A., TOMÉ, J. P., NEVES, M. G., TOMÉ, A. C., CAVALEIRO, J. A., CUNHA, Â. & ALMEIDA, A. 2013. Involvement of type I and type II mechanisms on the photoinactivation of non-enveloped DNA and RNA bacteriophages. *Journal of Photochemistry and Photobiology B: Biology,* 120**,** 10-16.

COSTA, L., FAUSTINO, M. A. F., NEVES, M. G. P., CUNHA, Â. & ALMEIDA, A. 2012. Photodynamic inactivation of mammalian viruses and bacteriophages. *Viruses,* 4**,** 1034-1074.

COSTA, L., TOMÉ, J. P., NEVES, M. G., TOMÉ, A. C., CAVALEIRO, J. A., FAUSTINO, M. A., CUNHA, Â., GOMES, N. C. & ALMEIDA, A. 2011. Evaluation of resistance development and viability

recovery by a non-enveloped virus after repeated cycles of aPDT. *Antiviral research,* 91**,** 278-282.
DAI, X., LI, Z., LAI, M., SHU, S., DU, Y., ZHOU, Z. H. & SUN, R. 2017. In situ structures of the genome and genome-delivery apparatus in a single-stranded RNA virus. *Nature,* 541**,** 112-116.
DAVIES, M. J. 2003. Singlet oxygen-mediated damage to proteins and its consequences. *Biochemical and Biophysical Research Communications,* 305**,** 761-770.
DEDEO, M. T., FINLEY, D. T. & FRANCIS, M. B. 2010. Viral capsids as self-assembling templates for new materials. *Progress in molecular biology and translational science,* 103**,** 353-392.
DOMINGO, E., ESCARMIS, C., SEVILLA, N., MOYA, A., ELENA, S., QUER, J., NOVELLA, I. & HOLLAND, J. 1996. Basic concepts in RNA virus evolution. *The FASEB Journal,* 10**,** 859-864.
DUFFY, S., SHACKELTON, L. A. & HOLMES, E. C. 2008. Rates of evolutionary change in viruses: patterns and determinants. *Nature reviews. Genetics,* 9**,** 267.
DULBECCO, R. & VOGT, M. 1954. PLAQUE FORMATION AND ISOLATION OF PURE LINES WITH POLIOMYELITIS VIRUSES. *The Journal of Experimental Medicine,* 99**,** 167-182.
FEIGELSTOCK, D. A., MIHALIK, K. B. & FEINSTONE, S. M. 2011. Selection of hepatitis C virus resistant to ribavirin. *Virology journal,* 8**,** 402.
FOLL, M., POH, Y.-P., RENZETTE, N., FERRER-ADMETLLA, A., BANK, C., SHIM, H., MALASPINAS, A.-S., EWING, G., LIU, P. & WEGMANN, D. 2014. Influenza virus drug resistance: a time-sampled population genetics perspective. *PLoS Genetics,* 10**,** e1004185.
GIULIANI, F., MARTINELLI, M., COCCHI, A., ARBIA, D., FANTETTI, L. & RONCUCCI, G. 2010. In vitro resistance selection studies of RLP068/Cl, a new Zn (II) phthalocyanine suitable for antimicrobial photodynamic therapy. *Antimicrobial Agents and Chemotherapy,* 54**,** 637-642.
GOENS, S. D., BOTERO, S., ZEMLA, A., ZHOU, C. E. & PERDUE, M. 2004. Bovine enterovirus 2: complete genomic sequence and molecular modelling of a reference strain and a wild-type isolate from endemically infected US cattle. *Journal of General Virology,* 85**,** 3195-3203.
GORZELNIK, K. V., CUI, Z., REED, C. A., JAKANA, J., YOUNG, R. & ZHANG, J. 2016. Asymmetric cryo-EM structure of the canonical Allolevivirus Qβ reveals a single maturation protein and the genomic ssRNA in situ. *Proceedings of the National Academy of Sciences,* 113**,** 11519-11524.
GRACANIN, M., PATTISON, D. I., HAWKINS, C. L. & DAVIES, M. J. 2007. Singlet oxygen-mediated photo-oxidation of tryptophan residues: Characterization of intermediate peroxides and stable products. *Free Radical Biology and Medicine,* 43**,** S126-S127.
HUÉ, S., GIFFORD, R. J., DUNN, D., FERNHILL, E., PILLAY, D. & RESISTANCE, U. C. G. O. H. D. 2009. Demonstration of sustained drug-resistant human immunodeficiency virus type 1 lineages circulating among treatment-naive individuals. *Journal of Virology,* 83**,** 2645-2654.
HUMPHREY, C. 2008. Negative Stain Transmission Electron Microscopy Quality Assessment of Viruses and Recombinant Virus-Like Particles. *Microscopy and Microanalysis,* 14**,** 166-167.
IRWIN, K. K., RENZETTE, N., KOWALIK, T. F. & JENSEN, J. D. 2016. Antiviral drug resistance as an adaptive process. *Virus evolution,* 2.
JAEGLE, M., BRIAND, J.-P., BURCKARD, J. & VAN REGENMORTEL, M. Accessibility of three continuous epitopes in tomato bushy stunt virus. Annales de l'Institut Pasteur/Virologie, 1988. Elsevier, 39-50.
JIMENEZ-CLAVERO, M., DOUGLAS, A., LAVERY, T., GARCIA-RANEA, J. & LEY, V. 2000. Immune recognition of swine vesicular disease virus structural proteins: novel antigenic regions that are not exposed in the capsid. *Virology,* 270**,** 76-83.
KAMINAKA, S., IMAMURA, Y., SHINGU, H., KITAGAWA, T. & TOYODA, T. 1999. Studies of bovine enterovirus structure by ultraviolet resonance Raman spectroscopy. *Journal of Virological Methods,* 77**,** 117-123.
KÄSERMANN, F. & KEMPF, C. 1997. Photodynamic inactivation of enveloped viruses by buckminsterfullerene1For the described inactivation procedure, a patent application was submitted.1. *Antiviral Research,* 34**,** 65-70.

KATPALLY, U., VOSS, N. R., CAVAZZA, T., TAUBE, S., RUBIN, J. R., YOUNG, V. L., STUCKEY, J., WARD, V. K., VIRGIN, H. W. & WOBUS, C. E. 2010. High-resolution cryo-electron microscopy structures of murine norovirus 1 and rabbit hemorrhagic disease virus reveal marked flexibility in the receptor binding domains. *Journal of Virology,* 84**,** 5836-5841.

KONING, R. I., GOMEZ-BLANCO, J., AKOPJANA, I., VARGAS, J., KAZAKS, A., TARS, K., CARAZO, J. M. & KOSTER, A. J. 2016. Asymmetric cryo-EM reconstruction of phage MS2 reveals genome structure in situ. *Nature communications,* 7.

KROPINSKI, A. M., MAZZOCCO, A., WADDELL, T. E., LINGOHR, E. & JOHNSON, R. P. 2009. Enumeration of bacteriophages by double agar overlay plaque assay. *Bacteriophages: Methods and Protocols, Volume 1: Isolation, Characterization, and Interactions***,** 69-76.

LAURING, A. S., FRYDMAN, J. & ANDINO, R. 2013. The role of mutational robustness in RNA virus evolution. *Nature reviews. Microbiology,* 11**,** 327.

LEWIS, J. K., BOTHNER, B., SMITH, T. J. & SIUZDAK, G. 1998. Antiviral agent blocks breathing of the common cold virus. *Proceedings of the National Academy of Sciences,* 95**,** 6774-6778.

LIU, Z.-Q., MAHMOOD, T. & YANG, P.-C. 2014. Western Blot: Technique, Theory and Trouble Shooting. *North American Journal of Medical Sciences,* 6**,** 160-160.

MAJIYA, H., ADEYEMI, O. O., STONEHOUSE, N. J. & MILLNER, P. 2018. Photodynamic inactivation of bacteriophage MS2: The A-protein is the target of virus inactivation. *Journal of Photochemistry and Photobiology B: Biology,* 178**,** 404-411.

MAJIYA, H., CHOWDHURY, K. F., STONEHOUSE, N. J. & MILLNER, P. 2017. TMPyP functionalised chitosan membrane for efficient sunlight driven water disinfection. *Journal of Water Process Engineering*.

PAYMENT, P., TREMBLAY, M. & TRUDEL, M. 1985. Relative resistance to chlorine of poliovirus and coxsackievirus isolates from environmental sources and drinking water. *Applied and Environmental Microbiology,* 49**,** 981-983.

PECSON, B. M., DECREY, L. & KOHN, T. 2012. Photoinactivation of virus on iron-oxide coated sand: Enhancing inactivation in sunlit waters. *Water Research,* 46**,** 1763-1770.

POURHAJIBAGHER, M., BOLUKI, E., CHINIFORUSH, N., POURAKBARI, B., FARSHADZADEH, Z., GHORBANZADEH, R., AZIEMZADEH, M. & BAHADOR, A. 2016a. Modulation of virulence in Acinetobacter baumannii cells surviving photodynamic treatment with toluidine blue. *Photodiagnosis and photodynamic therapy,* 15**,** 202-212.

POURHAJIBAGHER, M., CHINIFORUSH, N., SHAHABI, S., GHORBANZADEH, R. & BAHADOR, A. 2016b. Sub-lethal doses of photodynamic therapy affect biofilm formation ability and metabolic activity of Enterococcus faecalis. *Photodiagnosis and photodynamic therapy,* 15**,** 159-166.

PULLI, T., LANKINEN, H., ROIVAINEN, M. & HYYPIÄ, T. 1998. Antigenic Sites of Coxsackievirus A9. *Virology,* 240**,** 202-212.

REED, L. J. & MUENCH, H. 1938. A SIMPLE METHOD OF ESTIMATING FIFTY PER CENT ENDPOINTS 1 2. *American journal of epidemiology,* 27**,** 493-497.

SANJUAN, R., NEBOT, M. R., CHIRICO, N., MANSKY, L. M. & BELSHAW, R. 2010. Viral mutation rates. *Journal of Virology,* 84**,** 9733-9748.

SHEN, H. R., SPIKES, J. D., SMITH, C. J. & KOPECEK, J. 2000a. Photodynamic cross-linking of proteins - IV. Nature of the His-His bond(s) formed in the rose bengal-photosensitized cross-linking of N-benzoyl-L-histidine. *Journal of Photochemistry and Photobiology a-Chemistry,* 130**,** 1-6.

SHEN, H. R., SPIKES, J. D., SMITH, C. J. & KOPECEK, J. 2000b. Photodynamic cross-linking of proteins - V. Nature of the tyrosine-tyrosine bonds formed in the FMN-sensitized intermolecular cross-linking of N-acetyl-L-tyrosine. *Journal of Photochemistry and Photobiology a-Chemistry,* 133**,** 115-122.

SILVERMAN, A. I., PETERSON, B. M., BOEHM, A. B., MCNEILL, K. & NELSON, K. L. 2013. Sunlight Inactivation of Human Viruses and Bacteriophages in Coastal Waters Containing Natural Photosensitizers. *Environmental Science & Technology,* 47**,** 1870-1878.

SMYTH, M., TATE, J., HOEY, E., LYONS, C., MARTIN, S. & STUART, D. 1995. Implications for viral uncoating from the structure of bovine enterovirus. *Nature Structural & Molecular Biology,* 2**,** 224-231.

STONEHOUSE, N. & STOCKLEY, P. 1993. Effects of amino acid substitution on the thermal stability of MS2 capsids lacking genomic RNA. *FEBS letters,* 334**,** 355-359.

TAKAMATSU, H. & ISO, K. 1982. Chemical evidence for the capsomeric structure of phage Qbeta. *Nature,* 298**,** 819-824.

TAUBE, S., RUBIN, J. R., KATPALLY, U., SMITH, T. J., KENDALL, A., STUCKEY, J. A. & WOBUS, C. E. 2010. High-resolution x-ray structure and functional analysis of the murine norovirus 1 capsid protein protruding domain. *Journal of Virology,* 84**,** 5695-5705.

TAVARES, A., CARVALHO, C., FAUSTINO, M. A., NEVES, M. G., TOMÉ, J. P., TOMÉ, A. C., CAVALEIRO, J. A., CUNHA, Â., GOMES, N. & ALVES, E. 2010. Antimicrobial photodynamic therapy: study of bacterial recovery viability and potential development of resistance after treatment. *Marine drugs,* 8**,** 91-105.

VALEGÅRD, K., LILJAS, L., FRIDBORG, K. & UNGE, T. 1990. The three-dimensional structure of the bacterial virus MS2. *Nature,* 345**,** 36-41.

WAINWRIGHT, M. 2004. Photoinactivation of viruses. *Photochemical & Photobiological Sciences,* 3**,** 406-411.

WALDERICH, B., URSINUS-WÖSSNER, A., VAN DUIN, J. & HÖLTJE, J. V. 1988. Induction of the autolytic system of Escherichia coli by specific insertion of bacteriophage MS2 lysis protein into the bacterial cell envelope. *Journal of Bacteriology,* 170**,** 5027-5033.

WEBER, K. & OSBORN, M. 1969. The Reliability of Molecular Weight Determinations by Dodecyl Sulfate-Polyacrylamide Gel Electrophoresis. *Journal of Biological Chemistry,* 244**,** 4406-4412.

WILKINSON, F., HELMAN, W. P. & ROSS, A. B. 1995. Rate constants for the decay and reactions of the lowest electronically excited singlet state of molecular oxygen in solution. An expanded and revised compilation. *Journal of Physical and Chemical Reference Data,* 24**,** 663-677.

WITZ, J. & BROWN, F. 2001. Structural dynamics, an intrinsic property of viral capsids. *Archives of Virology,* 146**,** 2263-2274.

ZHANG, Y., ZHU, Y., GUPTA, A., HUANG, Y., MURRAY, C., VRAHAS, M., SHERWOOD, M., BAER, D., HAMBLIN, M. & DAI, T. 2014. Antimicrobial blue light therapy for multi-drug resistant Acinetobacter baumanni infection in mice: implications for prophylaxis and treatment of combat related infection. *J Infect Dis,* 17**,** 122-127.

ZHONG, Q., CARRATALÀ, A., NAZAROV, S., GUERRERO-FERREIRA, R. C., PICCININI, L., BACHMANN, V., LEIMAN, P. G. & KOHN, T. 2016. Genetic, Structural, and Phenotypic Properties of MS2 Coliphage with Resistance to ClO2 Disinfection. *Environmental Science & Technology,* 50**,** 13520-13528.

ZHONG, Q., CARRATALÀ, A., SHIM, H., BACHMANN, V., JENSEN, J. D. & KOHN, T. 2017. Resistance of Echovirus 11 to ClO2 Is Associated with Enhanced Host Receptor Use, Altered Entry Routes, and High Fitness. *Environmental Science & Technology,* 51**,** 10746-10755.